Analysis of Interactions Among Two Tropical Depressions and Typhoons Tembin and Bolaven (2012) in Pacific Ocean by Using Satellite Cloud Images

Ji-Chyun Liu, Yuei-An Liou, *Senior Member, IEEE*, Meng-Xi Wu, Yueh-Jyun Lee, Chi-Han Cheng, Ching-Pin Kuei, and Rong-Moo Hong

***Abstract*—This paper presents a framework for using remote sensing imagery and image processing techniques to analyze the interactions among tropical depressions (TDs) and typhoons. The purpose is to properly understand and predict this phenomenon, in order to reduce their influence on the regions where they pass by. Improvements on the understanding of the interactions among TDs and typhoons are obtained and presented. They carry the potential to improve forecast of severe weather system. In this paper, we analyzed the physical responses of TDs on two typhoons Tembin and Bolaven (2012), including TD's appearance, development, interaction, and mergence. According to the Central Weather Bureau of Taiwan, Tembin and Bolaven were formed about 1550 km apart. In general, the Fujiwhara effect happens when two storms are within a distance of 1400 km. Does the TD have impacts on the typhoons, and could we also call this impact as Fujiwhara effect? The 3-D profiles of the weather systems are reconstructed using the multifunctional transport satellite (MTSAT) infrared cloud images by the image reconstruction technique (IRT). The 3-D profiles of typhoons were implemented for investigating the in-depth distribution of the cloud top from a surface cloud image. The main parameters, which have been analyzed in this paper, are distance, height difference, rotation, and sizes of the two TDs and the two typhoons. The results showed that two TDs occurred between typhoons Tembin and Bolaven, which interacted with each other through upward convection and attraction between two typhoons and the TDs, respectively. The mergence of the two TDs caused the typhoons to start rotating and generate strengthened power. The findings of the TD effects on two typhoons represent a new aspect of the interaction between TD and typhoon.**

***Index Terms*—Satellite cloud image, three-dimensional (3-D) profile reconstruction, tropical depression (TD)–cyclone interaction.**

Manuscript received October 8, 2013; revised March 17, 2014; accepted June 28, 2014. The work of Y.-A. Liou was supported by the National Science Council under Grants NSC 101-221-E-008-019 and NSC 101-111-M-008-018.

J.-C. Liu, M.-X. Wu, C.-P. Kuei, and R.-M. Hong are with the Department of Electrical/Electronics Engineering, Chien Hsin University of Science and Technology, Zhongli 32097, Taiwan (e-mail: jichyun@cyu.edu.tw; cpkuei@uch.edu.tw).

Y.-A. Liou is with Center for Space and Remote Sensing Research, National Central University, Zhongli 32001, Taiwan (e-mail: yueian@csrsr.ncu.edu.tw).

Y.-J. Lee is with the Department of Information Management, Chien Hsin University of Science and Technology (previously Ching Yun University), Zhongli 32097, Taiwan (e-mail: yjlee@uch.edu.tw).

C.-H. Cheng is with the School of Hydrometeorology, Nanjing University of Information Science and Technology, Nanjing 210044, China (e-mail: herrymarry@gmail.com).

Digital Object Identifier 10.1109/TGRS.2014.2339220

I. Introduction

THE impacts of climate variability and global warming on the occurrence of tropical storms, including its distribution and variation, are valuable information for disaster prevention [1], [2]. The satellite data that provide cloud images may be used to analyze the cloud structure and the dynamics of typhoons [3], [4]–[9]. When two tropical cyclones (TCs) come close nearby (the distance between the cyclones generally less than 1400 km), they will affect each other and cause the rotation, which is so-called cyclone–cyclone interaction. The cyclone–cyclone interaction is also known as the "Fujiwhara effect" in honor of the pioneering work of Fujiwhara [10], who performed a series of laboratory experiments on the interactions between pairs of vortices in a water tank. There are several types of cyclone–cyclone interactions such as complete merge, partial merge (PM), complete straining out, partial straining out, and elastic interaction (EI) [11]. Recently, the interaction with different core vortex and sizes has been studied for understanding the nondivergent barotropic model [12], [13]. However, an argument question is still raised: does a Fujiwhara effect happen between the severe typhoons, if the distance between the two typhoons is more than 1500 km? Moreover, would the upward convection between TCs and TDs happen in addition to attraction if the TDs, which are smaller and lower than the TCs, appear between two cyclones and are located far from each other? Would the individual interactions among TD and TC, i.e., depression–cyclone interactions, cause the indirect two-cyclone interaction? These scientific questions lead to another issue: could we define the interaction between TD and TC as a new type of Fujiwhara effect?

In this paper, we present a case study that happened in the Pacific region east to Taiwan, to improve understanding of the Fujiwhara effect. It is our interpretation that the interaction of typhoon Tembin with Bolaven is an example of an indirect cyclone–cyclone interaction. On August 19, 2012, a tropical storm (Tembin) was formed in southeast of Taiwan, and at the same time, the other tropical storm (Bolaven) appeared in southwest of Mariana Islands. Two days later, the tropical storm Tembin maintained deep convective banding and tightly wrapped into a well-defined eye. Then, it moved to north-northwestward and located at the southeast of Taiwan. After reaching the southern tip of Taiwan on August 23, the typhoon

increased its intensity and made a dramatic U-turn. Finally, it approached the southern Taiwan on August 27. However, the tropical storm Bolaven moved west-northwestward, on August 21, and passed directly over Okinawa, on August 26, toward the north. Moreover, Bolaven began to interact with Tembin on August 25, caused it to execute a slow counterclockwise loop, and became stronger on August 26.

From August 21 to 26, the distance between the two typhoons was more than 1400 km, which is not supposed to be an ideal baseline distance, by most of the meteorologists, for having cyclone–cyclone interaction. However, our results showed that typhoons Tembin and Bolaven had interactions along the tracks of two typhoons. Hence, it is important to define or clearly recognize and locate two typhoons in this period of August 21–26, in particular, on the initial period of typhoon development. Due to the fact that the TD between these two typhoons existed in this period, the varieties of the two developing typhoons and the TD should be studied in this research.

The typhoon features have been studied, and analysis of various typhoon images is presented in this paper. The interactions include attraction, enhancement, PM, and merge among two typhoons and two TDs. Since the ice clouds or ice-covered surfaces on cloud were observed by using the shortwave infrared (SIR) channels [14]–[19], and based on cloud effective temperatures and optical depths with 3.7-[14] or 3.8-μm [18] detectors, they utilized a variety of empirical methods to crudely characterize the cloud vertical structure [18]. We also apply the SIR channel with 3.7 μm to detect the cloud images of typhoons to observe the cloud surfaces in depth. Due to the fact that the higher/larger typhoons and the lower/smaller TDs come close to each other, thus, the upward convection happens between typhoon and TD, and the depression–cyclone interactions occur. Therefore, except for the better visualization of the height changes among typhoon and TD, the image reconstruction technique (IRT) is employed to provide more information in the satellite images. Three parameters, including height difference, rotation, and size among two typhoons and TDs, have been used to expound TD–cyclone interaction, except the conventional parameter of distance. Finally, cloud images of typhoons, tracks of typhoons, 3-D profiles of typhoons, centers of typhoons, and time series of interactions have been used for present analysis. If more depression–cyclone interactions can be observed and quantified, it is very important for the weather prediction models and forecasts.

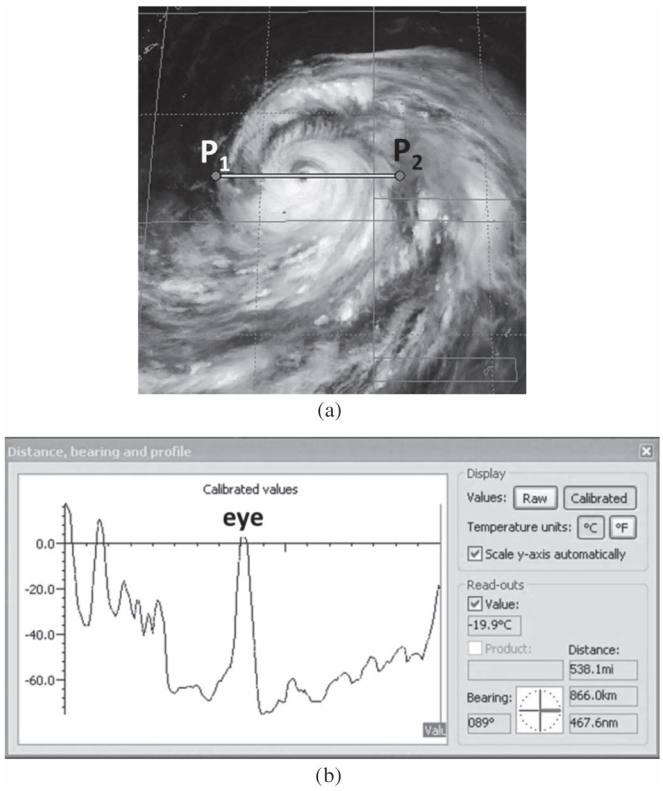

Fig. 1. Line profile with cloud top temperature. (a) Toggle profile mode with starting and stop points. (b) Distance, bearing, and profile window.

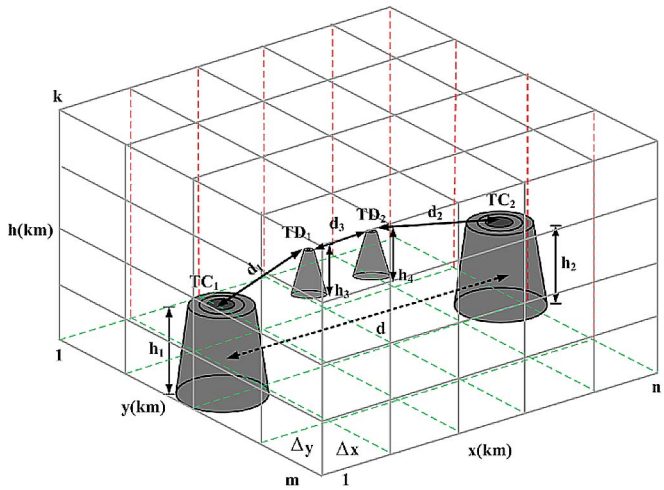

Fig. 2. Mesh-amplitude model applied for 3-D profiles of typhoon.

II. Three-Dimensional IRT

Three-dimensional profiles of typhoons were constructed using the IRT from the multifunctional transport satellite (MTSAT) cloud image data. The SIR channel with 3.7 μm was applied to detect the satellite cloud images of typhoons to observe the cloud surfaces in depth at first. A satellite cloud image was sliced in a vertical plane taking the line profile. The line profile was represented with cloud top temperature by toggling profile mode of integrated display and processing (iDAP) system [20] presented in Fig. 1(a) and (b). In Fig. 1(a), when the toggle profile mode is chosen, we click a point on the image to set the starting point (P_1) of a line and then determine the stop point (P_2). The distance, bearing, and profile window is obtained and display in Fig. 1(b). The window is a floating display. That is, it can be moved anywhere on the screen; the distance (horizontal axis) and temperature (vertical axis) will be presented in the Display and Read-out screen. This is a segmentation of the satellite cloud image sliced in a vertical plane. In the center of the line profile in Fig. 1(b), the sharp curve represents the in-depth display of the eye of typhoon. After slicing the cloud image in sequence, a series of vertical surfaces are produced for rendering the volume, as shown in Fig. 2. The mesh-amplitude model has been used to produce the structure of sliced plane from a satellite image and the 3-D

cloud images. Meanwhile, Fig. 2 presents the height variations under the conversion of the temperature.

The intensity of every pixel $P(x, y, h)$ in an image can be modeled as a function "Φ" of the neighboring pixels in space (x, y) and height (h), with assumption of causality, as follows:

$$P(x, y, h) = \Phi\left(P(x + \Delta x_i, y + \Delta y_j, h + \Delta h_k)\right) \quad (1)$$

where $(\Delta x_i, \Delta y_j, \Delta h_k)$ signify the neighborhood coverage in space and height. Equation (1) can be rewritten in terms of rows (x), columns (y), and heights(h) of a cloud image sequence as

$$T(x, y, h) = \sum_{k=h-K}^{h+K} \sum_{n=y-N}^{y+N} \sum_{m=x-M}^{x+M} W_{m,n,k} P(m, n, k). \quad (2)$$

In (2), the intensity of a pixel in an image as the weighted sum of the intensities of its neighboring pixels could be modeled. Here, m, n, and k correspond to the total number of rows, columns, and heights, respectively, and $W_{m,n,k}$ values are the corresponding cloud heights.

For a rectangular coordinate (x, y, h), the projective cloud image is located on the $x-y$ plane, and the height of typhoon is presented along the h-axis. The procedures are described as follows, with some assumptions.

- Step 1: When a typhoon occurs above the ocean, the ocean surface temperatures are taken as the reference and then the height difference is detected.
- Step 2: Cloud top temperature versus height conversion is 0.65 °C reducing per each 100-m height (the average adiabatic lapse ratio). Since the wet adiabatic lapse ratio (−0.55 °C/100 m) and the dry adiabatic lapse rate (−0.95 °C/100 m) are distributed from the bottom to the top of typhoons, the average adiabatic lapse ratio is used for approximation.
- Step 3: The $25 \times 25 (m \times n)$ mesh coordinate was shown in the mesh-amplitude model.
- Step 4: The line profile with cloud top temperature is sliced from the satellite cloud image data.
- Step 5: The 3-D profile of typhoon is reconstructed by the 19 (k) line profiles.
- Step 6: The profile of typhoon is an animation by rotating the coordinate.
- Step 7: Read the heights (h_1 and h_2) of number one (TC_1) and two (TC_2) typhoons, the heights (h_3 and h_4) of the TD_1 and TD_2, and the funnel depth of these typhoons.
- Step 8: Record the distances between the typhoons and the depressions on the top view of the 3-D profile, as shown in Fig. 3.

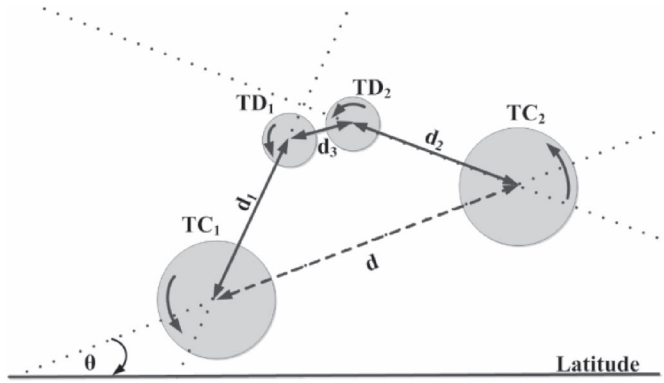

Fig. 3. Top view of 3-D profiles.

III. Analysis With Six-Day Cloud Images of Typhoons Tembin and Bolaven (2012)

Six-day cloud images of typhoons Tembin and Bolaven (2012) taken at 12:32, from August 21 to 26 (D_1–D_6), are shown in Fig. 4(a)–(f), respectively. The SIR (3.7 μm) channel is detected from the satellite cloud images with 1× 1 km pixel resolution. During the period of D_1–D_6, both typhoons Tembin and Bolaven separated apart, and the TD was observed at the same time, which is an important phenomenon in the cyclone–cyclone interaction process. The tracks of typhoons Tembin and Bolaven are plotted in Fig. 5. Typhoon Tembin went north and typhoon Bolaven went northwest within D_1–D_3. When the interaction occurs in D_3, the direction of typhoon Tembin was changed to the south with a U-turn, and typhoon Bolaven has been strengthened and accelerated toward north.

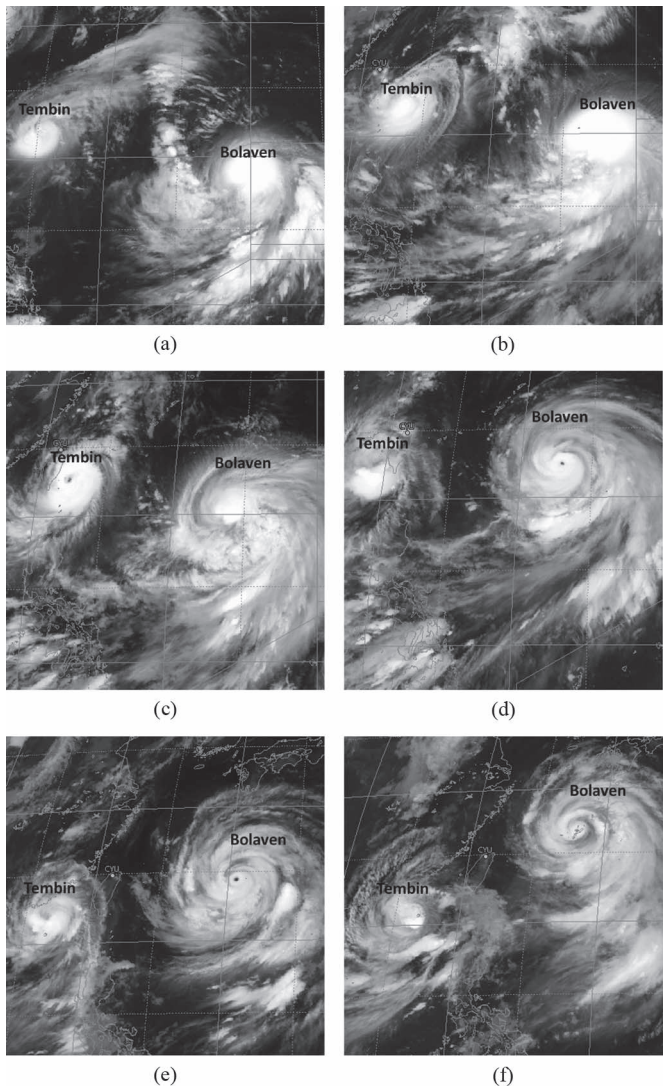

Fig. 4. Six-day cloud images of typhoons Tembin and Bolaven: (a) on D_1 = 12:32, August 21; (b) on D_2 = 12:32, August 22; (c) on D_3 = 12:32, August 23; (d) on D_4 = 12:32, August 24; (e) on D_5 = 12:32, August 25; (f) on D_6 = 12:32, August 26.

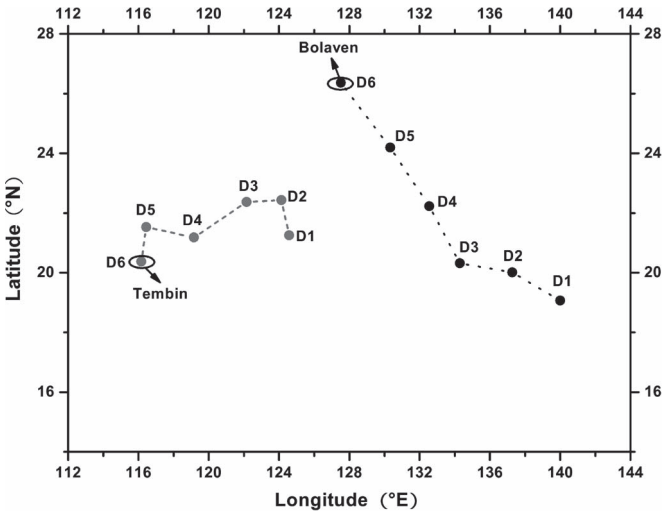

Fig. 5. Tracks of typhoons Tembin and Bolaven in the period of August 21–26.

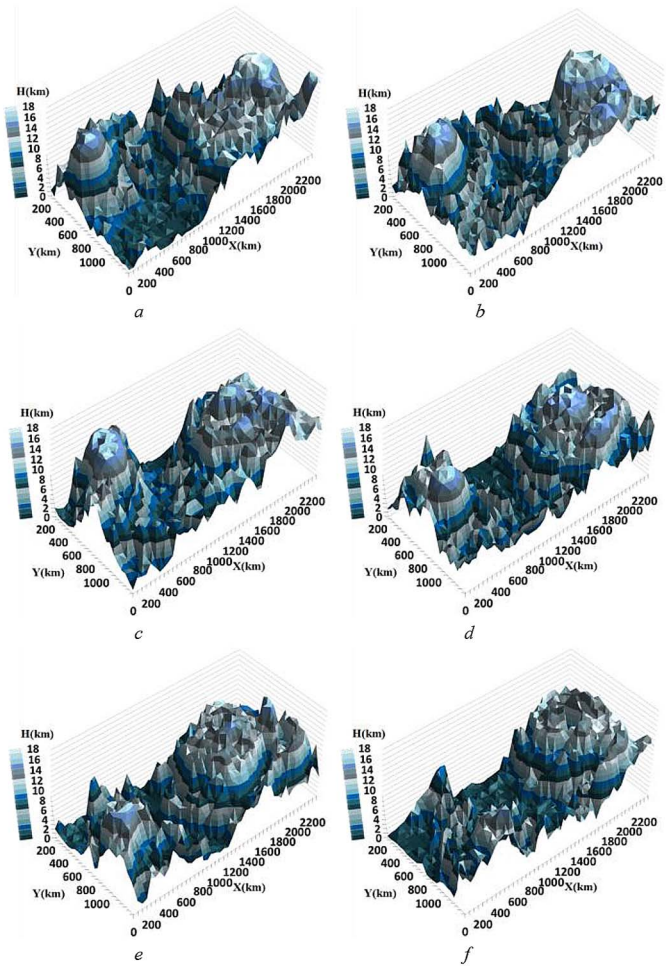

Fig. 6. Three-dimensional profiles of typhoons Tembin and Bolaven with 50° tilt and 45° rotation: (a) on D_1 = 12:32, August 21; (b) on D_2 = 12:32, August 22; (c) on D_3 = 12:32, August 23; (d) on D_4 = 12:32, August 24; (e) on D_5 = 12:32, August 25; and (f) on D_6 = 12:32, August 26.

The mesh-amplitude model and the graphical computer-aided design (CAD) (Excel 3-D plot) were applied to reconstruct the 3-D profiles of typhoons Tembin and Bolaven. Fig. 6(a) shows the 3-D profile of typhoons with 50° tilt and 45° rotations and the result of fixed cloud image in different

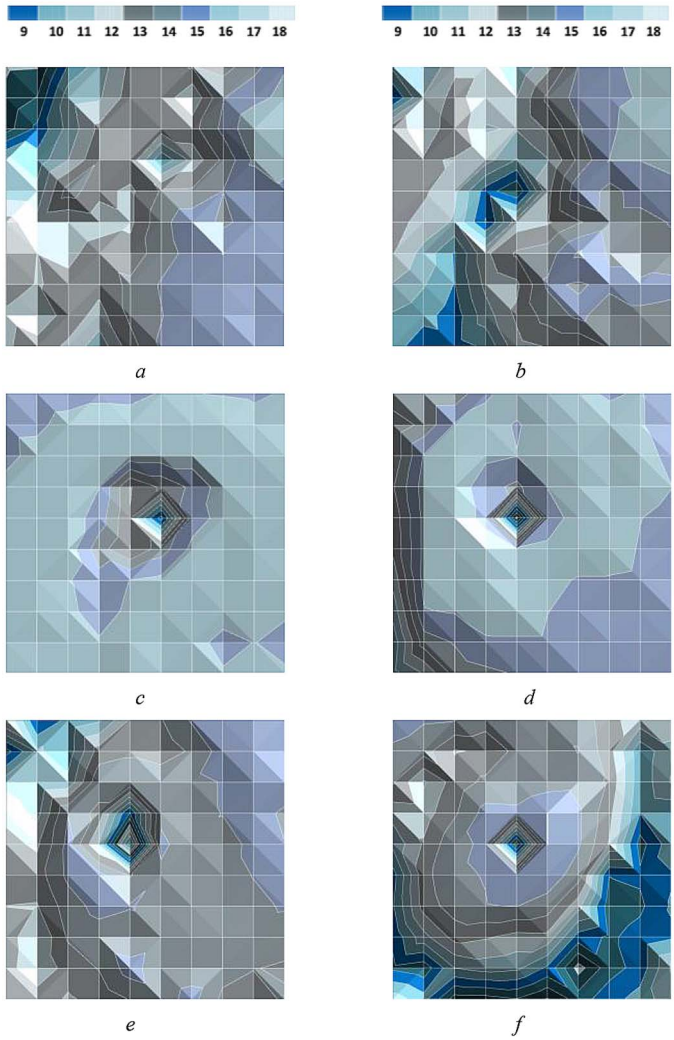

Fig. 7. Centers of typhoon Tembin: (a) on D_1 = 12:32, August 21; (b) on D_2 = 12:32, August 22; (c) on D_3 = 12:32, August 23. Centers of typhoon Bolaven: (d) on D_4 = 12:32, August 24; (e) on D_5 = 12:32, August 25; and (f) on D_6 = 12:32, August 26.

perspective of typhoons. With continuous increase in typhoon's tilt angle and rotation, Fig. 7(a) depicts the eyewall in the center of typhoon Tembin. Moreover, the 3-D profiles of typhoons from D_2 to D_6 are reconstructed. Fig. 6(b)–(f) illustrates the rotated 3-D profiles.

Fig. 7(a)–(f) shows the top views of the typhoons, which are similar to the land-form feature of the topographic map, where the eyewall is expressed at the center and presented with the decrement contours. Furthermore, the eyewall looks like a funnel and is assumed as the funnel effects in this study. Due to the fact that typhoon Tembin was stronger on D_1–D_3, its eyes and eyewalls were clear. Fig. 7(a) presents the funnel depth from top to bottom, and it is about 2.7 km. The larger funnels and eyes in the top view of typhoon Tembin, and two different eye sizes and funnel depths, are shown in Fig. 7(b) and (c), respectively. For D_4–D_6, typhoon Bolaven was stronger, and its eyes and eyewalls were clear. The eyes and eyewalls of typhoon Bolaven were observed and presented in Fig. 7(d)–(f), respectively. The eye sizes were 10 km × 10 km, 12 km × 8 km, and 8 km × 10 km, and funnel depths are about 10 km, 10 km, and

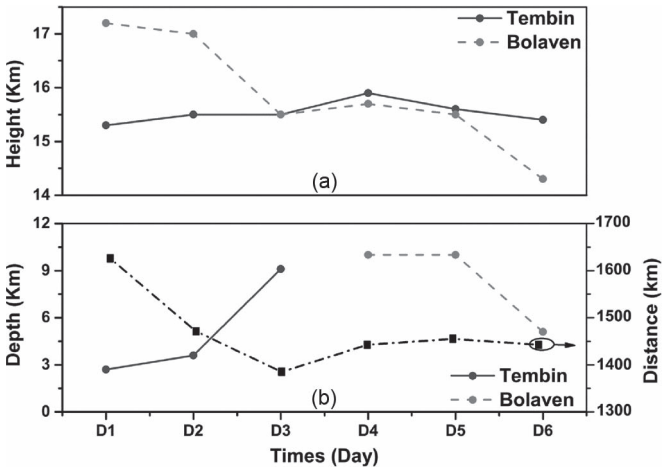

Fig. 8. Time series of interaction among typhoons Tembin and Bolaven on D1–D6. (a) Plotted with heights in six-day intervals. (b) Plotted with distances and funnel depths in six-day intervals.

5.1 km in Fig. 7(b) and (c), respectively. Obviously, typhoon Tembin was stronger on D_1–D_3 at first, and typhoon Bolaven was then strengthened on D_4–D_6.

It has been reported in the previous research work [6, Figs. 3(h), 4(h), and 5(h)] that, when the eye and eyewall convection are kept well, they can provide accurate information of track and intensity of the typhoon. The cloud images presented that the wreathed eye, the eye size, the central dense cloud region, and the screwy cloud band had been depicted the funnel shapes of the typhoon eyes. Furthermore, the gradients of the brightness temperatures sank into the center of the cloud image were shown in [3, Fig. 2(a)–(c)] and [4, Fig. 2(a)–(c)] of the previous works, and the variances of the distributions related to the wind speeds, which proved the funnel effects. However, both funnel depth and eye heights are mainly related to the intensity of the typhoon, but they have not been observed before.

By investigating Figs. 6(a)–(f) and 7(a)–(f), the heights and the funnel depths of the two typhoons are presented in Fig. 8(a) and (b), respectively. Fig. 8(a) depicts the height of the two typhoons, before and after their interaction. The height (h_1) of typhoon Tembin was 15.3 km, whereas the height (h_2) of typhoon Bolaven was 17.2 km. The height difference $(d = h_1 - h_2)$ was 2.1 km, on D_1. After interaction, the height of typhoon Tembin is varied slightly in the period of D_1–D_6, but the heights of typhoon Bolaven decrease successively from 17.2 to 14.2 km. Fig. 8(b) shows the distance of the two typhoons, before and after their interaction, as a function of time. The two typhoons on D_1 and D_2 started to interact at 1600- and 1470-km distances, respectively, and then, typhoons Tembin and Bolaven came close around 1400 km on D_3 and moved apart on D_4–D_6. Fig. 8(b) also exhibits the funnel depth of the two typhoons. The eyes and the eyewalls of typhoon Tembin are observed in the period of D_1–D_3, implying that typhoon Tembin was associated with a stronger cyclone with the values of 3.6–9.1 km, while typhoon Bolaven became stronger in the period of D_4–D_6 with the funnel depth varied, with the values of 5.1–10.0 km. According to the track in Fig. 5, the funnel depths in Fig. 8(a), and the height changes in Fig. 8(b), the interaction among typhoons Tembin and Bolaven might happen

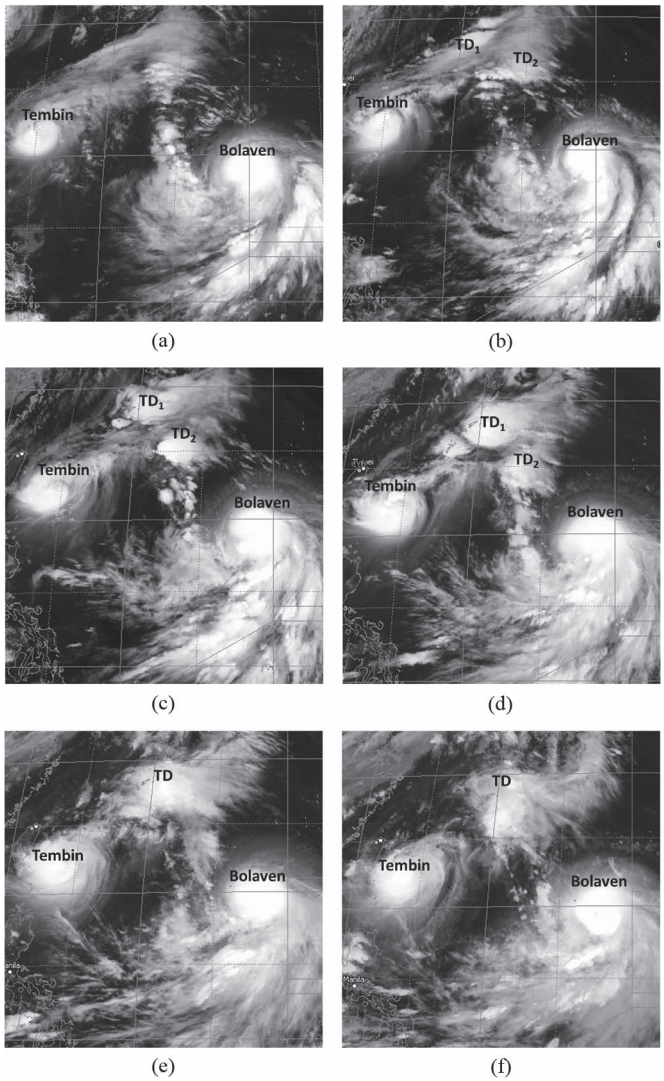

Fig. 9. Six-time cloud images of typhoons Tembin and Bolaven: (a) at $T_1 =$ 12:32, August 21; (b) at $T_2 =$ 17:32, August 21; (c) at $T_3 =$ 21:32, August 21; (d) at $T_4 =$ 01:32, August 22; (e) at $T_5 =$ 05:32, August 22; and (f) at $T_6 =$ 09:32, August 22.

on D_3. However, the distances between typhoons Tembin and Bolaven are more than 1400 km; in Fig. 8(b), it is above the baseline distance of Fujiwhara effect; thus, it does not belong to the Fujiwhara effect. Before D_3, the TDs appear and were observed in the period of D_1–D_2, as shown in Fig. 4(a) and (b); the typhoons could be under the influence of TDs. The TDs between the two typhoons in the period of D_1–D_2 should be studied and clarified.

IV. Detailed Analysis With Six-Time Cloud Images of Typhoons Tembin and Bolaven (2012)

Fig. 9(a)–(f) shows the six-time cloud images of typhoons Tembin and Bolaven taken from August 21 to 22 at different time periods. During the period of T_1–T_6, the movements of both typhoons Tembin and Bolaven were slow. In Fig. 9(a), it is evident that TD_1 appears between typhoon Tembin and Bolaven, while the development of TD_2 is evident in Fig. 9(b). Therefore, the two TDs formed in the period of T_3–T_4 are

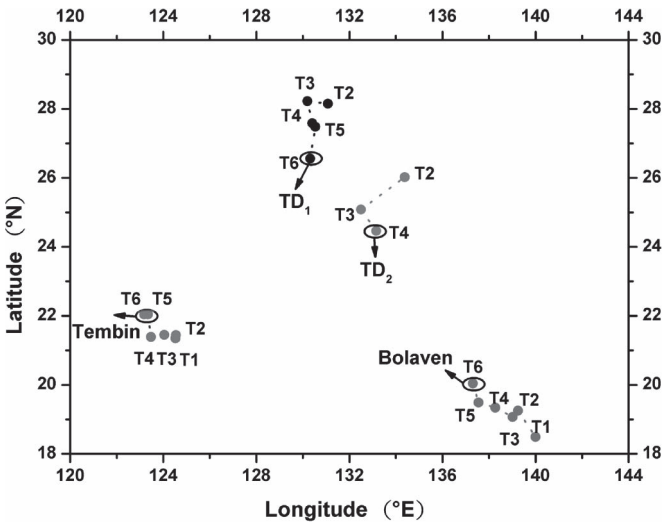

Fig. 10. Tracks of typhoons Tembin and Bolaven and two TDs in the period of August 21–22.

shown in Fig. 9(c) and (d). The interaction between typhoon Tembin and TD_1 and that between typhoon Bolaven and TD_2 could be found by inspecting convection between them. Therefore, two sets of depression–cyclone interactions occur, and they could be assumed as a combined depression–cyclone interaction. During the period of T_5–T_6, TD_1 and TD_2 merged together and formed a new TD. This newly formed TD provides convection to two typhoons Tembin and Bolaven, as shown in Fig. 9(e) and (f). The tracks of typhoons Tembin and Bolaven are plotted in Fig. 10. Typhoon Tembin moved toward west, while the typhoon Bolaven moved toward northwest, within T_1–T_6. Both TD_1 and TD_2 occurred in T_2. The direction of the movement of TD_1 changed counterclockwise to the south after interacting with typhoon Tembin within T_2–T_6. On the other hand, the direction of the movement of TD_2 was changed counterclockwise and was directed to typhoon Bolaven within T_2–T_4. Thus, the two sets of depression–cyclone interactions can be demonstrated.

The mesh-amplitude model and the graphical CAD were combined to reconstruct the 3-D profiles of typhoons Tembin and Bolaven in six-time intervals. Fig. 11(a)–(f) shows the 3-D profiles of typhoons with 50° tilt and 45° rotations. The distance between typhoons Tembin and Bolaven, between Tembin and TD_1, and between Bolaven and TD_2 are demonstrated in Fig. 12(a). Moreover, the heights of typhoon Tembin and TD_1, as well as Bolaven and TD_2, are presented in Fig. 12(b) and (c), respectively. In Fig. 12(a), the distances between typhoons Tembin and Bolaven are within 1500–1600 km. However, it is said that cyclone–cyclone interaction would not occur if the distance between two cyclones is more than 1400 km. Considering the existence of the TDs, typhoon Tembin and TD_1 located about 910–980 km apart, at T_2–T_6, and Bolaven and TD_2 came close about 780–920 km apart, at T_2–T_4. Obviously, two individual depression–cyclone interactions happened. Although we do not have the exact answer, it is definitely interesting to find out if the TD makes the typhoon do a U-turn. Nevertheless, two sets of depression–cyclone interactions occur due to the closer distances. Fig. 12(b) and (c) presents typhoon Tembin indirectly interacting with typhoon Bolaven through the two depression–cyclone interactions and the merge of TD_1 and

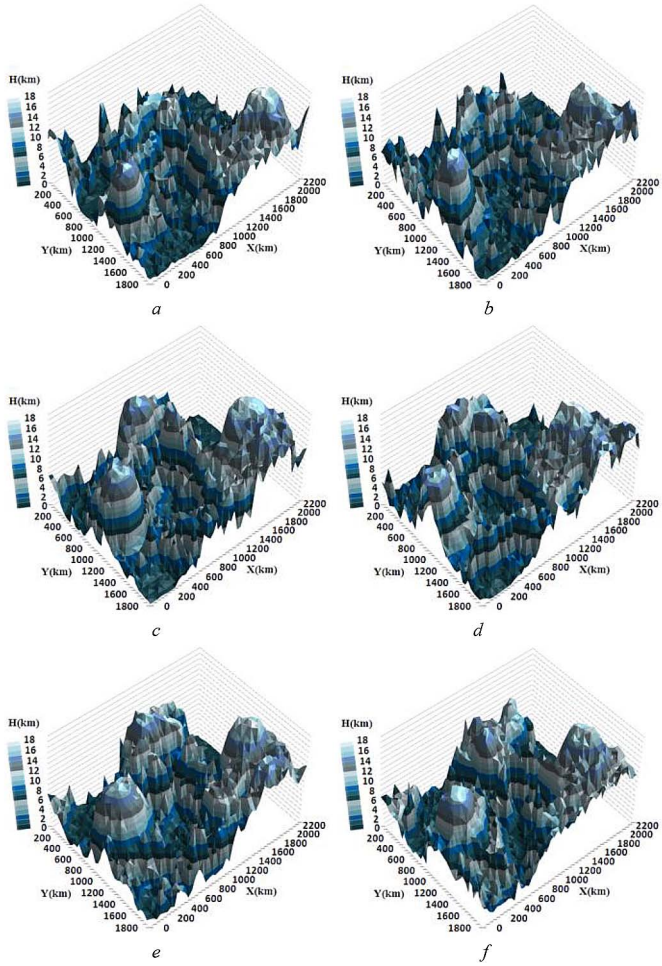

Fig. 11. Three-dimensional profiles of typhoons Tembin and Bolaven with 50° tilt and 45° rotation: (a) at T1 = 12:32, August 21; (b) at T2 = 17:32, August 21; (c) at T3 = 21:32, August 21; (d) at T4 = 01:32, August 22; (e) at T5 = 05:32, August 22; and (f) at T6 = 09:32, August 22.

TD_2. The height (h_1) of typhoon Tembin (TC_1) was about 14.5–15.9 km in the periods of T_1–T_6, while the height (h_3) of TD_1 was about 12 km at T_1, and TD_1 then moved up step by step to 14.8 km at T_6. The attraction, upward convection, and PM between Tembin and TD_1 can be observed. For example, in Fig. 12(c), the height (h_2) of typhoon Bolaven (TC_2) was about 17.3–17.5 km in the periods of T_1–T_6, and the height of TD_2 was about 12.5 km at T_2. TD_2 was drawn up in the period of T_3 and T_4. Finally, the attraction, upward convection and PM between Bolaven and TD_2 can be also seen, and TD_2 was merged into TD at the end. In Fig. 12(d), the varied sizes of typhoons and TDs are presented. Two sets of depression–cyclone interactions occurred in the period of T_2–T_4. The interaction between typhoon Tembin and TD_1 caused the former to diminish and the later to enlarge. On the other hand, the interaction between typhoon Bolaven and TD_2 results the former to enhance and the latter to diminish. After the mergence of TD_1 and TD_2 into TD, TD interacts with both typhoons and provides upward convections in the periods of T_5–T_6. Therefore, typhoons Tembin and Bolaven are linked together and interact with each other. Due to the larger size of typhoon Bolaven, typhoon Tembin was changed to the south with a U-turn, and typhoon Bolaven has been strengthened and accelerated toward the north.

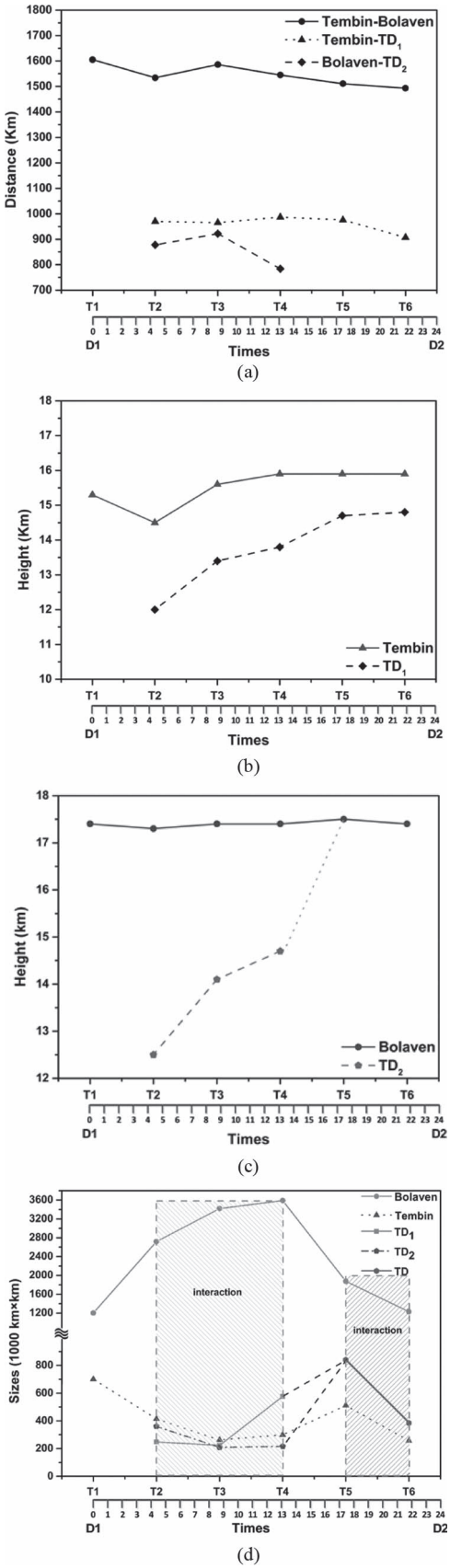

Fig. 12. Time series of interaction among typhoons Tembin and Bolaven and TDs in T1–T6. (a) Plotted with distances in six-time intervals. (b) Plotted with heights of typhoon Tembin and TD1 in six-time intervals. (c) Plotted with heights of typhoon Bolaven and TD2 in six-time intervals. (d) Plotted with sizes of typhoons Tembin and Bolaven and TDs in six-time intervals.

In summary, an individual depression–cyclone interaction happened at the distance of 1000 km between typhoon Tembin and TD_1, with a height difference of 2 km and with counterclockwise rotation. The other interaction occurred at the distance of 900 km between typhoon Bolaven and TD_2, with a height difference of 3.5 km and with counterclockwise rotation. The long-distance typhoon–typhoon interaction possibly occurs through the two sets of depression–cyclone interactions and the subsequent merging of TD_1 and TD_2. Therefore, typhoon Tembin indirectly interacts with typhoon Bolaven. Meanwhile, the influence of the two TDs on the two typhoons is an alternative approach to depict the interaction of two typhoons even apart more than 1400-km distance.

V. Summary and Conclusion

The 3-D profile of the IRT was used to develop the mesh-amplitude model for interpreting the depression–cyclone interaction. To produce a mesh-amplitude model, the line profiles with cloud top temperature sliced from the satellite cloud image data were constructed. After slicing the cloud image in sequence, a series of the vertical surfaces for volume are rendered, as shown in Fig. 1. Next, sample six-day cloud images of typhoons Tembin and Bolaven (2012) were depicted in Fig. 3(a)–(f), for analysis. The tracks of typhoons Tembin and Bolaven were plotted in Fig. 4. The 3-D profiles of typhoons Tembin and Bolaven were developed by using the mesh-amplitude model when the samples and tracks were determined. Meanwhile, in Fig. 6(a)–(f), the eyes in the center of typhoons Tembin and Bolaven became bigger. The distances of typhoons Tembin and Bolaven were shown in Fig. 7(a), the heights of two typhoons were presented in Fig. 7(b), and the funnel depths of the two typhoons were listed in Fig. 7(c). The results in Fig. 8(a)–(c) were used to analyze the interaction of typhoons Tembin and Bolaven. Finally, for detailed analysis and depicting the depression–cyclone interaction, six-time cloud images of typhoons Tembin and Bolaven and the TDs are shown in Fig. 9(a)–(f). The tracks of typhoons and TDs were plotted in Fig. 10. The 3-D profiles of typhoons and TD were shown in Fig. 11(a)–(f). The time series of depression–cyclone interactions were presented in Fig. 12(a)–(d).

The four parameters analyzed and discussed in the present work, including distance, height difference, rotation, and size, can be very good indicators in understanding the depression–cyclone interactions. The 3-D profile of the IRT clarified the combination of depression–cyclone interactions and TD merges. Due to the fact that higher/larger typhoons Tembin and Bolaven and the lower/smaller TD had come close to each other, the two sets of depression–cyclone interactions existed in the processing. Typhoon Tembin has increased in intensity and made a U-turn, and Bolaven was intensified and changed its direction by the effect of combined interactions. It is an alternative cyclone–cyclone interaction (Fujiwhara effect), which designated the long-distance cyclone–cyclone interactions. The long-distance cyclone–cyclone interaction could happen when the mid-TD located within two cyclones and the two cyclones are with the distance more than 1400 km. The funnel effect presented in the center of typhoon can be

expressed by the strength of the typhoons. Therefore, in future work, if more long-distance cyclone–cyclone interactions are observed and quantified, the relationship between the funnel effect and the typhoon intensity may be even better interpreted.

REFERENCES

[1] M. M. Gierach and B. Subrahmanyam, "Satellite data analysis of the upper ocean response to hurricanes Katrina and Rita (2005) in the Gulf of Mexico," *IEEE Geosci. Remote Sens. Lett.*, vol. 4, no. 1, pp. 132–136, Jan. 2007.

[2] J. Acker *et al.*, "Interaction of hurricane Katrina with optically complex water in the Gulf of Mexico: Interpretation using satellite-derived inherent optical properties and chlorophyll concentration," *IEEE Geosci. Remote Sens. Lett.*, vol. 6, no. 2, pp. 209–213, Apr. 2009.

[3] M. F. Piñeros, E. A. Ritchie, and J. S. Tyo, "Objective measures of tropical cyclone structure and intensity change from remotely sensed infrared image data," *IEEE Trans. Geosci. Remote Sens.*, vol. 46, no. 11, pp. 3574–3580, Nov. 2008.

[4] M. F. Piñeros, E. A. Ritchie, and J. S. Tyo, "Estimating tropical cyclone intensity from infrared image data," *Weather Forecast.*, vol. 26, no. 5, pp. 690–698, Oct. 2011.

[5] C. C. Wu, "Numerical simulation of typhoon Gladys (1994) and its interaction with Taiwan terrain using the GFDL hurricane model," *Mon. Weather Rev.*, vol. 129, no. 6, pp. 1533–1549, Jun. 2001.

[6] C. J. Zhang and X. D. Wang, "Typhoon cloud image enhancement and reducing speckle with genetic algorithm in stationary wavelet domain," *IET Image Process.*, vol. 3, no. 4, pp. 200–216, Aug. 2009.

[7] I. F. Pun, I. I. Lin, C. R. Wu, D. S. Ko, and W. T. Liu, "Validation and application of altimetry-derived upper ocean thermal structure in the western North Pacific Ocean for typhoon-intensity forecast," *IEEE Trans. Geosci. Remote Sens.*, vol. 45, no. 6, pp. 1616–1630, Jun. 2007.

[8] C. Liu, T. Y. Shyu, C. C. Chao, and Y. F. Lin, "Analysis on typhoon Long Wang intensity changes over the ocean via satellite data," *J. Mar. Sci. Technol.*, vol. 17, no. 1, pp. 23–28, 2009.

[9] C. A. Somporn *et al.*, "3D cloud and storm reconstruction from satellite image," in *Modeling, Simulation and Optimization of Complex Processes*. Berlin, Germany: Springer-Verlag, 2008, pp. 187–206.

[10] S. Fujiwhara, "On the growth and decay of vortical systems," *Q. J. R. Meteorol. Soc.*, vol. 49, no. 206, pp. 75–104, Apr. 1923.

[11] R. Prieto, B. D. McNoldy, S. R. Fulton, and W. A. Schubert, "A classification of binary tropical cyclone-like vortex interactions," *Mon. Weather Rev.*, vol. 131, no. 11, pp. 2656–2666, Nov. 2003.

[12] C. C. Wu, T. S. Huang, W. P. Huang, and K. H. Chou, "A new look at the binary interaction: Potential vorticity diagnosis of the unusual southward movement of typhoon Bopha (2000) and its interaction with typhoon Saomai (2000)," *Mon. Weather Rev.*, vol. 131, no. 7, pp. 1289–1300, Jul. 2003.

[13] Y. J. Joung, M. K. Lin, Y. C. Lin, C. W. Chang, and H. H. A. Chen, "A simulation of Fujiwhara effect on a structured agent-based peer-to-peer system," in *Proc. 2nd Int. Conf. Commun. Syst. Softw. Middleware Workshops*, 2007, pp. 1–7.

[14] S. Platnick *et al.*, "The MODIS cloud products: Algorithms and examples from Terra," *IEEE Trans. Geosci. Remote Sens.*, vol. 41, no. 2, pp. 459–473, Feb. 2003.

[15] M. D. King *et al.*, "Cloud and aerosol properties, precipitable water, profiles of temperature and humidity from MODIS," *IEEE Trans. Geosci. Remote Sens.*, vol. 41, no. 2, pp. 442–458, Feb. 2003.

[16] H. L. Huang *et al.*, "Inference of ice cloud properties from high spectral resolution infrared observations," *IEEE Trans. Geosci. Remote Sens.*, vol. 42, no. 4, pp. 842–853, Apr. 2004.

[17] G. Hong *et al.*, "The sensitivity of ice cloud optical and microphysical passive satellite retrievals to cloud geometrical thickness," *IEEE Trans. Geosci. Remote Sens.*, vol. 45, no. 5, pp. 1315–1323, May 2007.

[18] P. Minnis *et al.*, "CERES Edition 2 cloud property retrievals using TRMM VIRS and Terra and Aqua MODIS data: Part I: Algorithms," *IEEE Trans. Geosci. Remote Sens.*, vol. 49, no. 11, pp. 4374–4400, Nov. 2011.

[19] P. Minnis *et al.*, "CERES Edition-2 cloud property retrievals using TRMM VIRS and Terra and Aqua MODIS Data—Part II: Examples of average results and comparisons with other data," *IEEE Trans. Geosci. Remote Sens.*, vol. 49, no. 11, pp. 4401–4430, Nov. 2011.

[20] [Online]. Available: http://www.dartcom.co.uk/products/lrit_hrit/idap_macropro/index.php

Ji-Chyun Liu was born in Taiwan, in 1951. He received the B.S., M.S., and Ph.D. degrees from the Chung Cheng Institute of Technology, Taoyuan, Taiwan, in 1974, 1981, and 1993, respectively.

From 1981 to 2003, he was an Instructor, Associate Professor, and Professor with the Chung Cheng Institute of Technology. Since 2003, he has been a Professor with Chien Hsin University of Science and Technology, Zhongli, Taiwan. His research interests include microwave integrated circuit design, wideband filter, wideband amplifier, chaotic oscillator, broadband antenna, fractal antenna, active integration antenna, broadband absorber, ceramic metamaterial, electromagnetic inteference/electromagnetic compatibility, and microwave instrumentation and measurement.

Yuei-An Liou (S'91–M'96–SM'01) received the B.S. degree in electrical engineering (EE) from the National Sun Yat-Sen University (NSYSU), Kaohsiung, Taiwan, in 1987 and the M.S.E. degree in EE, the M.S. degree in atmospheric and space sciences, and the Ph.D. degree in EE and atmospheric, oceanic, and space sciences from the University of Michigan, Ann Arbor, MI, USA, in 1992, 1994, and 1996, respectively.

From 1989 to 1990, he was a Research Assistant with the Robotics Laboratory, National Taiwan University, Taipei, Taiwan. From 1991 to 1996, he was a Graduate Student Research Assistant with the Radiation Laboratory, University of Michigan, where he developed land–air interaction and microwave emission models for prairie grassland. He joined the Faculty of the Center for Space and Remote Sensing Research (CSRSR) in 1996 and the Institute of Space Sciences in 1997 at the National Central University (NCU), Zhongli, Taiwan, where he is now a Distinguished Professor. In 2005, he was the Division Director with the Science Research Division, National Space Organization (NSPO), Taiwan, where he continued to serve as an Advisor in 2006. From August 2006 to July 2007, he was a Chair Professor and Dean of the College of EE and Computer Science, Chien Hsin University of Science and Technology, Zhongli, Taiwan. From 2007 to 2010, he was the Director of CSRSR, NCU. He has over 100 referral papers and more than 200 international conference papers. His current research activities include GPS meteorology and ionosphere; remote sensing of the atmosphere, land surface, and polar ice; and land surface process modeling.

Dr. Liou is a Principal Investigator on many research projects sponsored by the Ministry of Science and Technology (MOST), the Council of Agriculture, NSPO, the Civil Aeronautics Administration, the Minister of Interior, the Water Conservancy Agency of Taiwan, and the Office of Naval Research of USA. He serves as a Referee for many journals, including *Terrestrial, Atmospheric and Oceanic Sciences*; IEEE TRANSACTIONS ON GEOSCIENCE AND REMOTE SENSING (TGRS); *International Journal of Remote Sensing*; *Earth, Planets, and Space*; *Water Resources Research*; *Remote Sensing of Environment*; *J. Geophys. Res.*; *Annales Geophysicae.* He has been a member of the Editorial Advisory Board for *GPS Solutions*, since 2001; *International Journal of Navigation and Observation*, since 2011; InTech Scientific Board (Environmental Sciences) for 2011/2014; *Pakistan Journal of Meteorology*, since 2013. He has served as an Editor for the *Journal of Aeronautics, Astronautics and Aviation* since 2009; as an Associate Editor for the IEEE JOURNAL OF SELECTED TOPICS IN APPLIED EARTH OBSERVATIONS AND REMOTE SENSING (JSTARS) since 2008 and *Remote Sensing Technology and Application* since 2011; and as the Editor-in-Chief for *Remote Sensing Open* since 2014. In addition, he is the Lead Guest Editor for special issues (*GPS Solutions* in 2005 and 2010; IEEE TGRS in 2008; *Advances in Meteorology* and *Terrestrial, Atmospheric and Oceanic Sciences* in 2014). He has been the President of the Taiwan Group on Earth Observations since 2010 and the President of the University of Michigan Alumni Association in Taiwan since 2012. He is listed in Who's Who in the World. He was a recipient of Annual Research Awards from the National Science Council (NSC), in 1998, 1999, and 2000; a recipient of The First Class Research Awards from the NSC, in 2004, 2005, and 2006; and a recipient of the NCU Outstanding Research Awards in 2004, 2006, 2007, and 2008. He was awarded the "Contribution Award to FORMOSAT3 National Space Mission" by NSPO, in 2006. He is a member of the American Geophysical Union, the American Meteorological Society, and the International Association of Hydrological Sciences. He was awarded Honorary Life Member of The Korean Society of Remote Sensing, in 2007. He was elected Foreign Member of the Russian Academy of Engineering Sciences, in 2008. He was awarded Outstanding Alumni Awards by the University of Michigan Alumni Association in Taiwan and NSYSU, in 2008. He was elected as an Academician by the International Academy of Astronautics in 2009. He was honored as a Distinguished Professor by NCU, in 2010 and 2013. He was awarded the Golden Prize by NSYSU in 2013.

Meng-Xi Wu was born in Taiwan, in 1987. He received the B.S. degrees from Ching Yun University, Zhongli, Taiwan, in 2010. He is currently working toward the M.A. degree with the Chien Hsin University of Science and Technology, Zhongli, Taiwan.

His research interest includes microwave circuit design, wideband filter, wideband amplifier, antenna design, and measurement.

Yueh-Jyun Lee was born in Taiwan, in 1960. He received the B.S., M.S., and Ph.D. degrees from the Chung Cheng Institute of Technology, Taoyuan, Taiwan, in 1982, 1988, and 1997, respectively.

He is currently an Assistant Professor with the Chien Hsin University of Science and Technology, Zhongli, Taiwan. His research interests include computer network, neural network, digital logic circuit design, and embedded system.

Chi-Han Cheng was born in Taiwan, in 1980. He received the B.S. degree in civil engineering from the Chung Yuan Christian University, Zhongli, Taiwan, in 2002; the M.S. degree in hydrological sciences from the National Central University, Zhongli, Taiwan, in 2004; and the Ph.D. degree in civil, environmental, and construction engineering from the University of Central Florida, Orlando, FL, USA, in 2012.

He is currently an Associate Professor with the Nanjing University of Information Science and Technology, Nanjing, China. His research interests include hydroclimatic extremes: drought monitoring and analysis, land use impacts on energy and water balances, and hydrology remote sensing.

Ching-Pin Kuei was born in I-lan, Taiwan, in 1953. He received the B.S. degree in physics from the Chung Cheng Institute of Technology, Taoyuan, Taiwan, in 1975 and the M.S. and Ph.D. degrees in electrical engineering from the University of Michigan, Ann Arbor, MI, USA, in 1984 and 1988, respectively.

He is currently an Associate Professor with the Chien Hsin University of Science and Technology, Zhongli, Taiwan. His research interests include photovoltaics, microwave measurement, absorbers, and filters.

Rong-Moo Hong was born in Taiwan, in 1957. He received the B.S. degree in physics from the Chung Cheng Institute of Technology, Taoyuan, Taiwan, in 1980; the M.S. degree in physics from the National Taiwan University, Taipei, Taiwan, in 1985; and the Ph.D. degree in photoelectron engineering from the Ecole Central de Nantes, Nantes, France, in 1996.

He is currently an Associate Professor with the Chien Hsin University of Science and Technology, Zhongli, Taiwan. His research interests include photovoltaics, light-emitting diode and LD devices, and laser applications.